Geology of diamond occurrences at southern Knee Lake, Oxford Lake–Knee Lake greenstone belt, Manitoba (NTS 53L14, 15)

S.D. Anderson (Manitoba Geological Survey)

Summary and guide to figures

In 2016, bedrock mapping and sampling by the Manitoba Geological Survey resulted in the discovery of microdiamonds in shoreline outcrop at southern Knee Lake – a discovery since confirmed and extended by Altius Minerals Corp. (press release, September 25, 2017). The microdiamonds are hosted by polymictic volcanic conglomerate and volcanic sandstone belonging to the Oxford Lake group (ca. 2.72 Ga) of the Oxford Lake–Knee Lake greenstone belt in the northwestern Superior province (**Figures 1–5**). Well-preserved primary features (**Figures 6–8**) indicate deposition as debris and turbidity flows in an alluvial or shallow-marine fan setting, whereas interlayers of lapilli tuff (**Figure 9**) record influxes of pyroclastic material.

Whole-rock geochemical data (**Figures 10 & 11**) indicate primitive bulk compositions (16.7–18.7 wt. % MgO; >500 ppm Cr, Ni) and alkaline affinities (1.2–3.3 wt. % K_2O) for the volcanic sandstone and lapilli tuff, collectively referred to as the 'ultramafic facies association', and are comparable to primitive alkaline lamprophyre dikes in the Knee Lake area (**Figure 12**), suggesting an association with lamprophyric volcanism.

Diverse clast types in the conglomerate include pyroxenite, gabbro and basalt, presumably derived from the ca. 2.83 Ga Hayes River group (**Figure 13**), representing the local basement. Distinctive cored clasts (**Figure 14**) in the diamondiferous conglomerate are interpreted to represent pelletal lapilli that formed during intensive degassing within a diatreme vent and were subsequently reworked by sedimentary processes.

Multiphase ductile deformation fabrics (**Figures 15 & 16**), greenschist-facies metamorphic assemblages, and interstratification with dacitic volcanic rocks dated at 2722 ± 3 Ma (**Figures 5 & 17**) confirm the Archean emplacement age, placing this diamond occurrence amongst the oldest known on Earth.

Indicator minerals in the conglomerate (MGS sample LX/KL-2) consist of chromite and Cr-spinel, whereas the lapilli tuff (MGS sample LX/KL-3) contains chromite, Cr-diopside, Cr-spinel and diamond-inclusion Cr-spinel, indicative of a mantle-derived magmatic precursor sourced from within the diamond stability field (>140 km depth). Indicator mineral compositions (**Figures 18 & 19**), coupled with the absence of garnet and ilmenite, suggest that the magmatic precursor was not kimberlitic.

Microdiamonds (n = 144; **Figures 20 & 21**) obtained from a 15.8 kg sample of the volcanic conglomerate (sample LX/KL-2) are variable in colour, morphology and degree of resorption, with the largest stone weighing 0.2071 mg (0.00104 ct); a sample of the lapilli tuff did not yield diamonds, whereas lamprophyre dikes at Knee Lake have yet to be assessed for diamonds or indicator minerals.

Unconventional diamond occurrences hosted by lamprophyre dikes, polymict volcaniclastic breccia and conglomerate in the Michipicoten greenstone belt (south-central Superior province) near Wawa, Ontario, provide a useful analog to the occurrence at southern Knee Lake, with implications for exploration.

As is the case in the Wawa area, the types and compositions of indicator minerals hosted by the lamprophyric rocks at Knee Lake are distinctly different from those found in surficial sediments. The former are compatible with 'typical' mantle-derived rocks such as komatiite or primitive arc basalt, which are major constituents of greenstone belts in the Superior province, whereas the latter are indicative of diverse sources, possibly including kimberlite. Consequently, any exploration strategy that employs drift prospecting will require careful consideration of not only the complex surficial geology and ice-transport history in the Knee Lake region, but also the potentially diverse and extensive sources of indicator minerals.

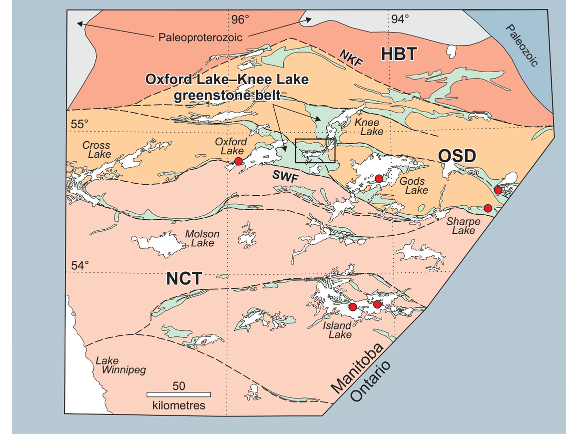

Figure 1: Regional geological setting of the Oxford Lake–Knee Lake greenstone belt in the northwestern Superior province (terminology after Stott et al., 2010). Significant gold deposits are indicated by red circles. Abbreviations: HBT, Hudson Bay terrane; NCT, North Caribou terrane; NKF, North Kenyon fault; OSD, Oxford–Stull domain; SWF, Stull-Wunnummin fault. Location of **Figure 2** is outlined.

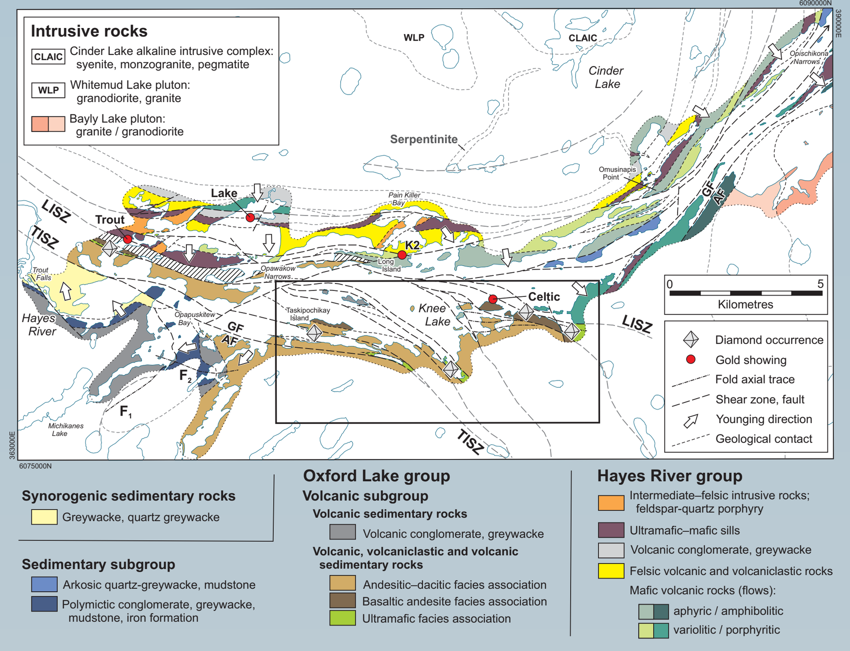

Figure 2: Simplified geology of southern Knee Lake (after Anderson et al., 2015a), including diamond occurrences reported by Anderson (2017b) and Altius Minerals Corp. (press release, September 25, 2017). Geology outside the mapping limit is simplified from Gilbert (1985) and high-resolution aeromagnetic data. Hachure pattern indicates undivided tectonite. Abbreviations: AF and GF indicate structural boundaries between amphibolite facies and greenschist facies rocks; LISZ, Long Island shear zone; TISZ, Taskipochikay Island shear zone. Location of **Figure 3** is outlined.

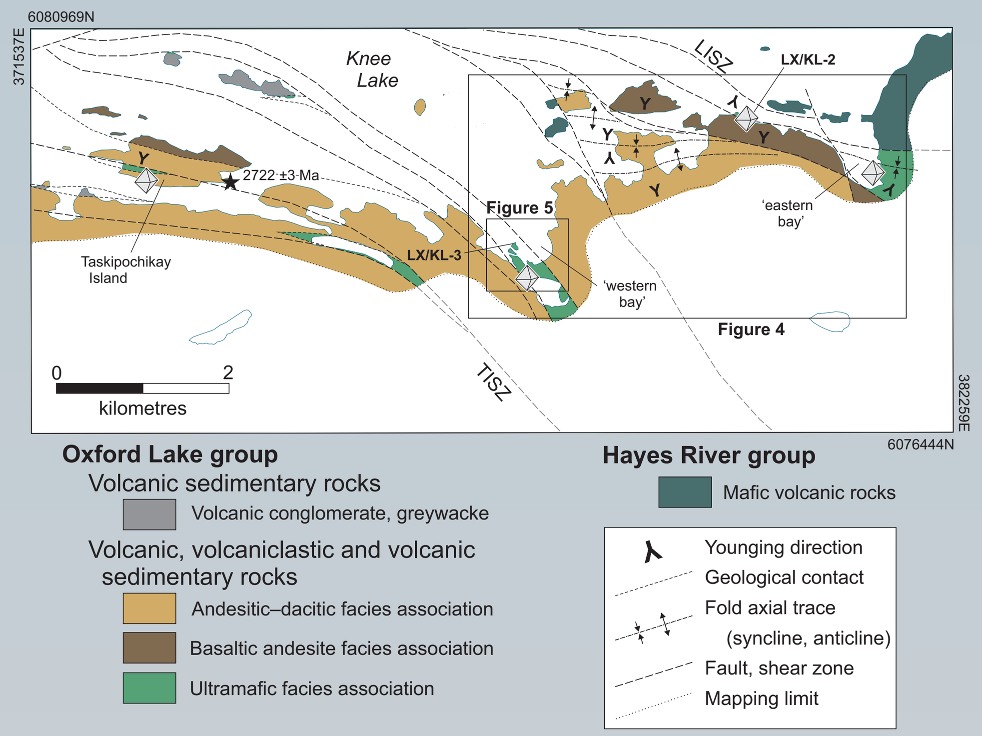

Figure 3: Simplified geology of southeastern Knee Lake showing the distribution of the ultramafic facies association (UFA) and the locations of the western and eastern bays (type localities of the UFA). Also shown are the locations of MGS samples LX/KL-2 and LX/KL-3, and diamond occurrences reported by Altius Minerals Corp.

Locations of **Figure 4** and **Figure 5** are outlined.

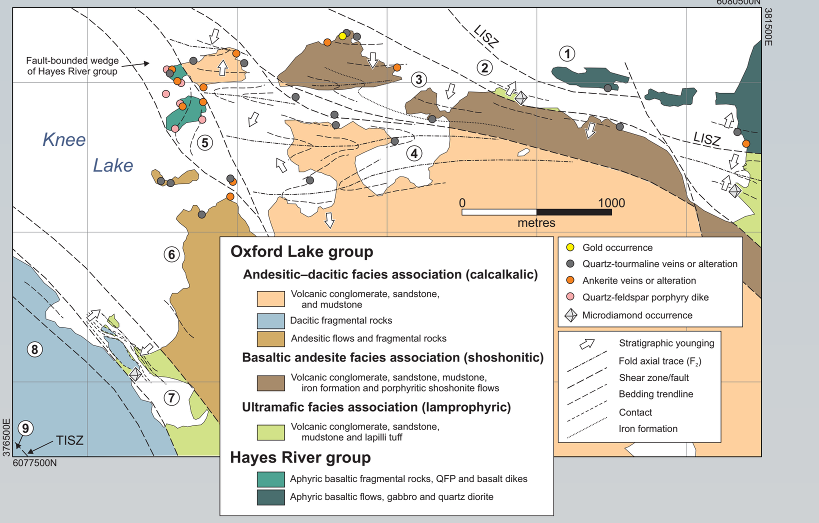

Figure 4: Revised geology of the southeastern portion of southern Knee Lake (Anderson, 2017a). Numbers (1–9) indicate major, fault-bounded, lithostructural panels. Abbreviations: LISZ, Long Island shear zone; QFP, quartz-feldspar porphyry; TISZ, Taskipochikay Island shear zone. Microdiamonds have been recovered from the ultramafic facies association in panels 2 and 7.

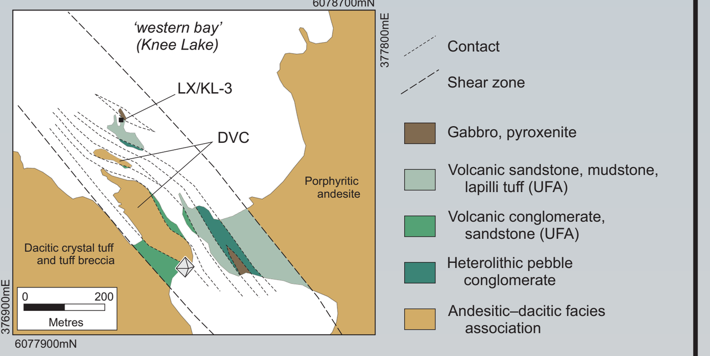

Figure 5: Detailed map of the western bay (Anderson, 2017b) showing thick lenses of dacitic volcanic conglomerate (DVC) of the andesitic–dacitic facies association (2722 Ma; Corkery et al., 2000) interstratified with the ultramafic facies association (UFA). Diamond occurrence as reported by Altius Minerals Corp.

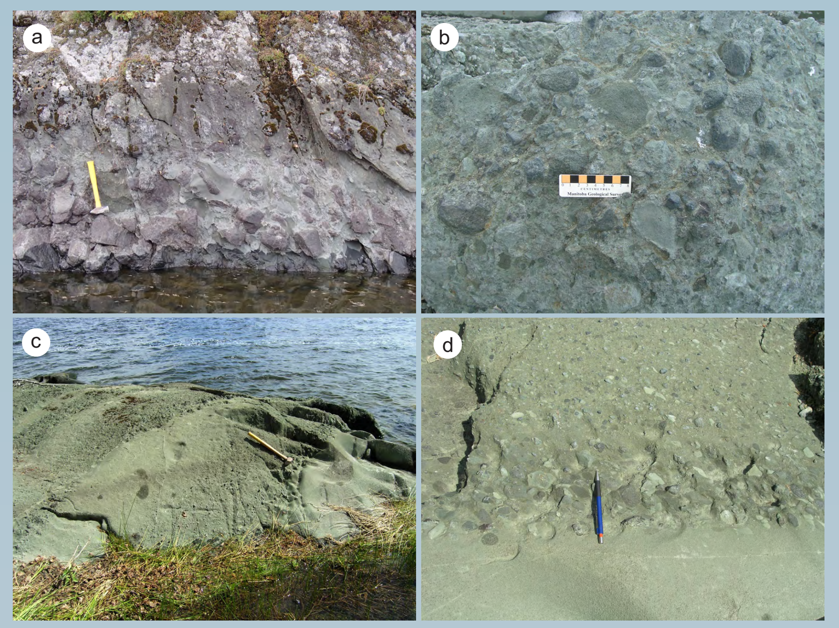

Figure 6: Outcrop photographs of diamondiferous polymictic conglomerate of the UFA: a) boulder–cobble conglomerate, western bay; b) massive cobble–pebble conglomerate showing polymictic clast population and rounded clasts, eastern bay; c) cobble–pebble conglomerate beds at the discovery outcrop (MGS sample LX/KL-2 locality) showing size grading and deeply scoured basal contacts, eastern bay; d) detail of graded bed of polymictic conglomerate, discovery outcrop, eastern bay.

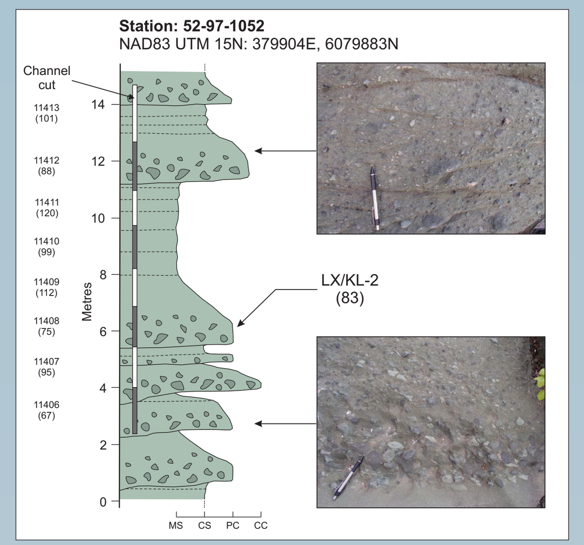

Figure 7: Simplified stratigraphic column for bedded polymictic conglomerate at the discovery outcrop in the eastern bay. Normally-graded beds are capped by pebbly sandstone, consistent with sedimentation from high-density turbidity currents. Channel samples are from Altius Minerals Corp. (press release, September 25, 2017), following up on the original MGS sample (LX/KL-2). Numbers in parentheses indicate diamond counts in the +0.106 mm size fractions (note higher counts in sandy beds). Abbreviations: CC, cobble conglomerate; CS, coarse-grained sandstone; MS, medium-grained sandstone; PC, pebble conglomerate.

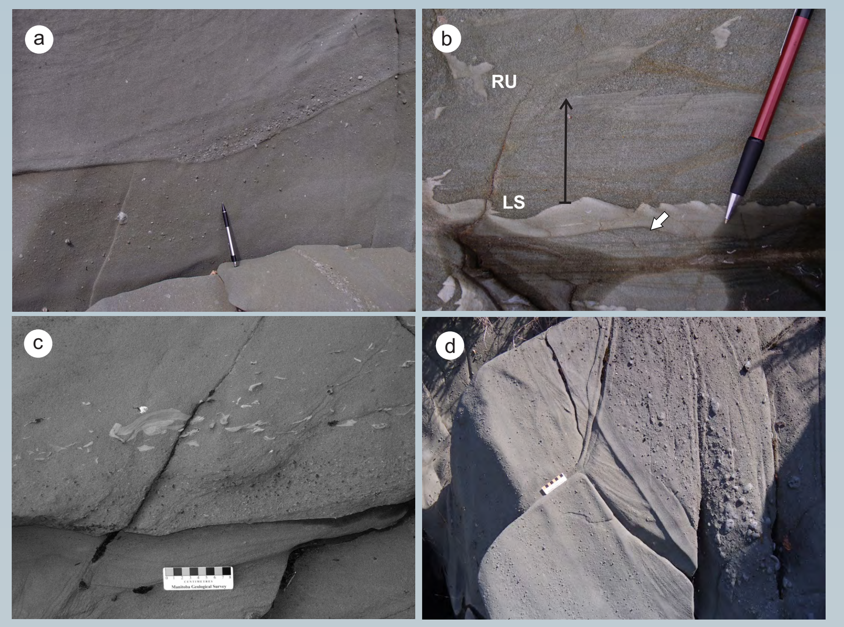

Figure 8: Outcrop photographs of sandstone in the UFA: a) pebbly sandstone showing scour-and-fill channel at the base and convolute bedding at the top, eastern bay; b) turbiditic sandstone and mudstone, showing normal size-grading (black arrow), load structures (LS), ripples (arrow) and mudstone rip-ups (RU), western bay; bedding is overturned in this location; pencil points north; c) normally-graded sandstone bed with contorted rip-ups of mudstone, eastern bay; d) diffuse compound size-grading and cross-bedding in pebbly sandstone and conglomerate, eastern bay.

Figure 9: Outcrop photographs of lapilli tuff (MGS sample LX/KL-3 locality) in the western bay: a) matrix-supported lapilli tuff showing the essentially monolithic character (gabbro clast indicated by arrow); b) detail of lapillus showing ragged margin and vesicular texture.

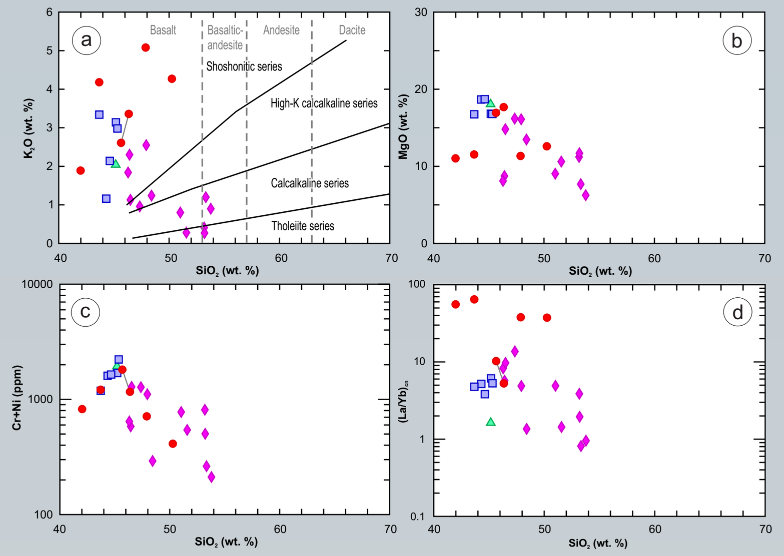

Figure 10: Whole-rock geochemical data for various components of the UFA (sandstone, blue squares; lapilli tuff, green triangle; clasts in conglomerate, purple diamonds), including for comparison purposes examples of primitive lamprophyre dikes from Oxford Lake and Knee Lake (red circles; grey tie-lines indicate the most primitive dikes); a) SiO_2 vs. K_2O; fields for shoshonitic, high-K calcalkaline, calcalkaline and tholeiitic series are from Peccerillo and Taylor (1976); b) SiO_2 vs. MgO; c) SiO_2 vs. sum of Cr+Ni; d) SiO_2 vs. (La/Yb)cn (cn, chondrite normalized; values of Sun and McDonough, 1989). Diagrams illustrate the compositional similarity of the volcanic sandstone, lapilli tuff and the primitive lamprophyre dikes.

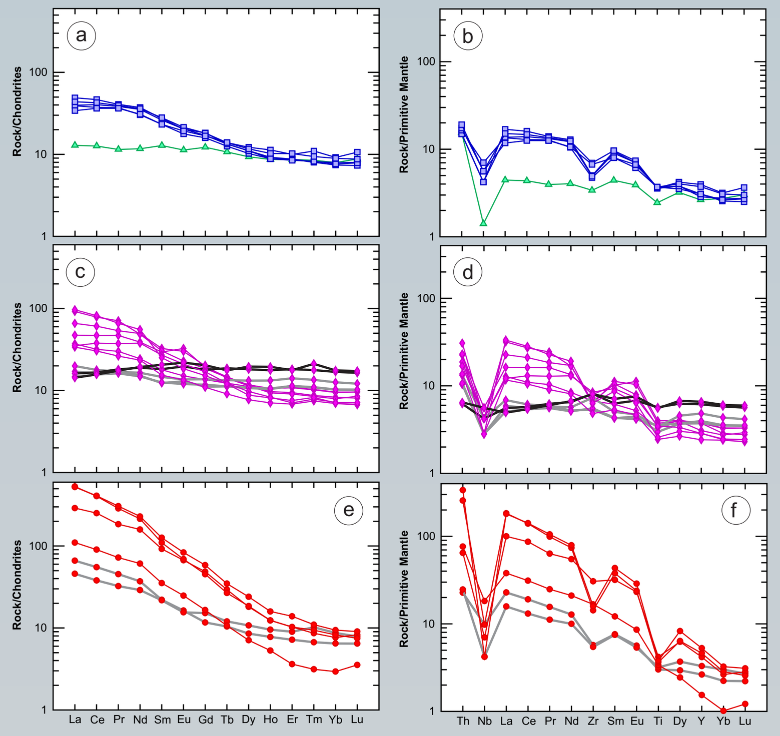

Figure 11: Chondrite and primitive mantle–normalized trace-element diagrams for the various components of the UFA, including for comparison purposes examples of lamprophyre dikes from Oxford Lake and Knee Lake (symbols as in **Figure 10**); a) and b) sandstone and lapilli tuff; c) and d) clasts in conglomerate (different coloured tie-lines indicate the three different profiles evident in this sample set); e) and f) lamprophyre dikes (grey tie-lines indicate the most primitive dikes). Normalizing values are from Sun and McDonough (1989).

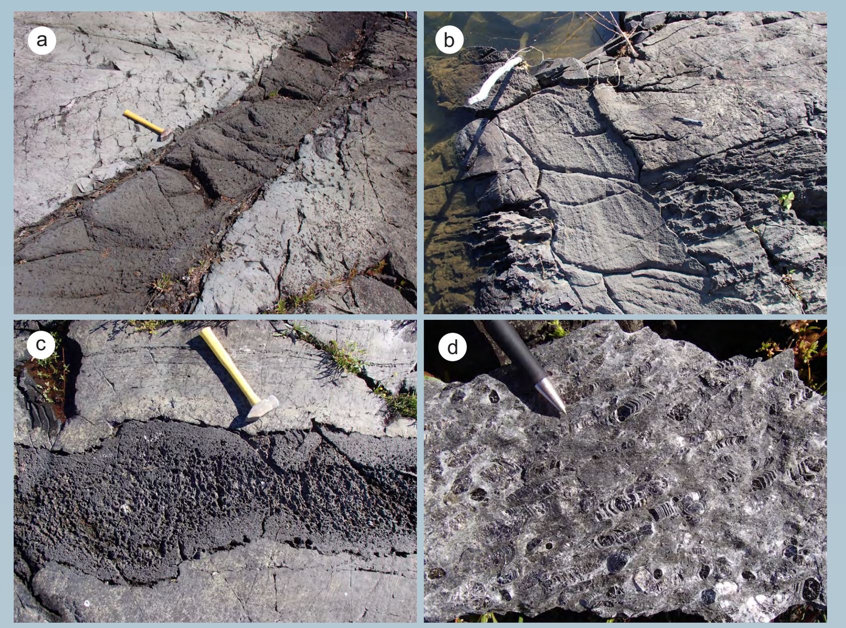

Figure 12: Outcrop photographs of lamprophyre dikes at central Knee Lake: a) primitive (11 wt. % MgO) lamprophyre dike; b) flow-banded dike of more evolved lamprophyre (7.7 wt. % MgO); c) primitive (11.5 wt. % MgO) lamprophyre dike with thick chilled margins; d) coarse phenocrysts of phlogopite in primitive lamprophyre dike (same locality as previous photo).

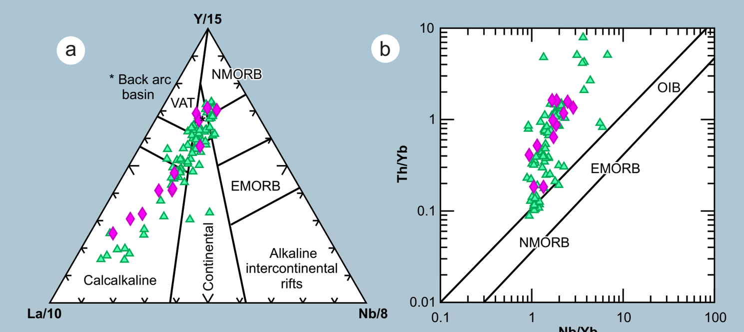

Figure 13: Trace element discrimination diagrams for clasts in conglomerate of the UFA (purple diamonds), shown in comparison to mafic volcanic rocks of the HRG at Oxford Lake and Knee Lake, representing the local basement during alkaline volcanism (green triangles; unpublished data from Syme et al., 1997, 1998; Anderson et al., 2012, 2013): a) La/10 vs. Y/15 vs. Nb/8 (Cabanis and Lecolle, 1989); b) Log Nb/Yb vs. Log Th/Yb (Pearce and Peate, 1995). Abbreviations: EMORB, enriched mid-ocean–ridge basalt; NMORB, normal mid-ocean–ridge basalt; OIB, ocean-island basalt; VAT, volcanic-arc tholeiite.

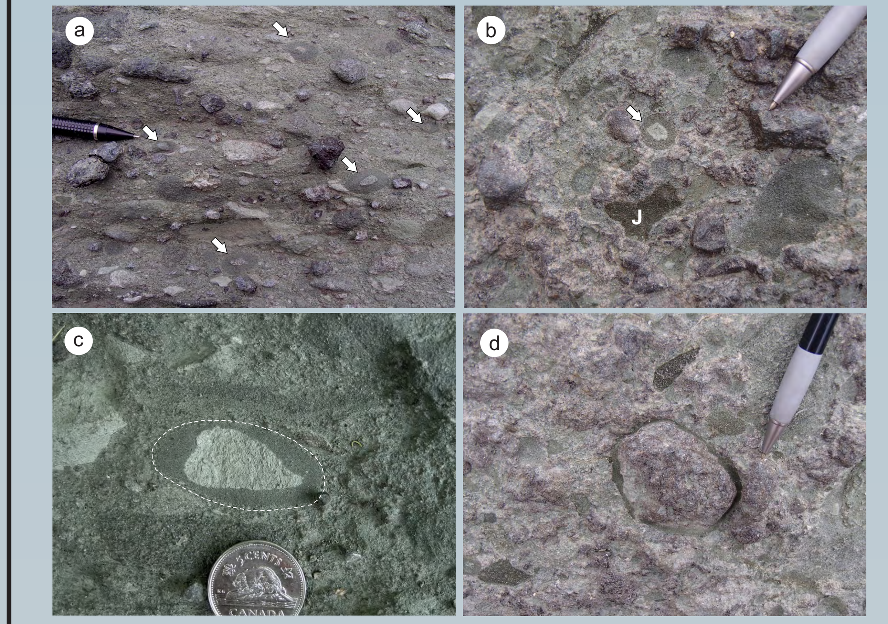

Figure 14: Outcrop photographs of pelletal lapilli from diamondiferous conglomerate in the eastern bay: a) pebble conglomerate bed containing abundant pelletal lapilli (arrows); b) pelletal lapilli (arrow) and dark green clasts of juvenile lithic material (J); c) detail of lapillus (dashed outline), showing serpentinite core and lithic rim; d) large lapillus showing thin continuous rim of dark green lithic material around a pyroxenite core.

Figure 15: Outcrop photographs of deformation structures at southern Knee Lake, based on the deformation sequence of Anderson et al. (2015b) and Anderson (2016): a) isoclinal F_1 fold, defined by iron formation in greywacke ('S_0' indicates bedding), overprinted by F_2 folds (axial planes are indicated by dashed lines); b) steep L_2 stretching lineation in conglomerate; prolate fabric indicated by aspect ratios of clasts on the horizontal and vertical outcrop faces; c) bedding-parallel S_1 foliation and isoclinal F_2 fold in the UFA, western bay; d) vertical outcrop face showing steep stretching lineation (L_2) at a high-angle to bedding in the hinge of a mesoscopic F_2 fold in the UFA, western bay; e) shallow-plunging L_4 stretching lineation defined by deformed clasts in volcanic conglomerate; f) mylonitic S_4 foliation and F_4 Z-folds in the Long Island shear zone (asymmetric quartz boudins indicate dextral shear).

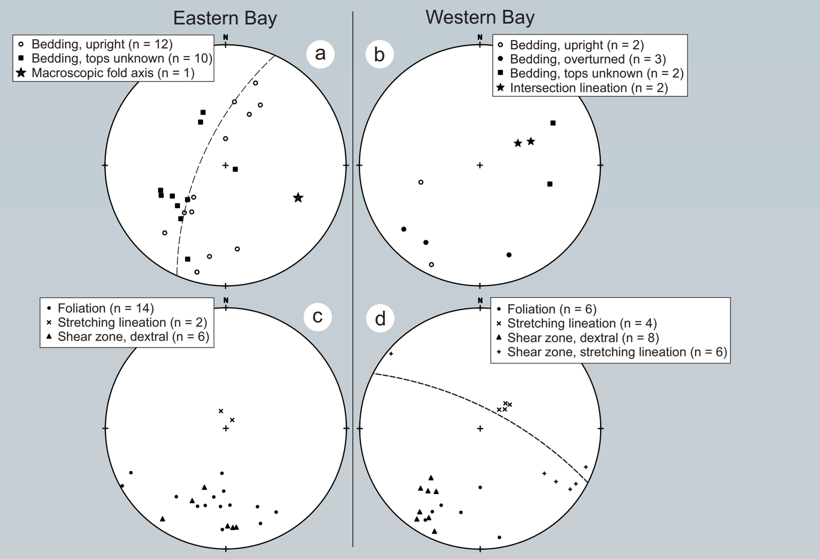

Figure 16: Lower-hemisphere, equal-angle stereographic projections of structural data from the UFA: a) poles to bedding in the eastern bay; star represents pole to girdle (dashed line) defined by bedding orientations and indicates the plunge of a macroscopic F_2 fold (star); b) poles to bedding (S_0) in the western bay; stars indicate measured S_0-S_2 intersection lineations, corresponding to mesoscopic F_2 fold hinges; c) L_2 lineation and poles to planar fabrics (foliation is S_2; shear zones are S_4) in the eastern bay; d) L_2 (steep) and L_4 (shallow) lineations and poles to planar fabrics (foliation is S_2; shear zones are S_4) in the western bay.

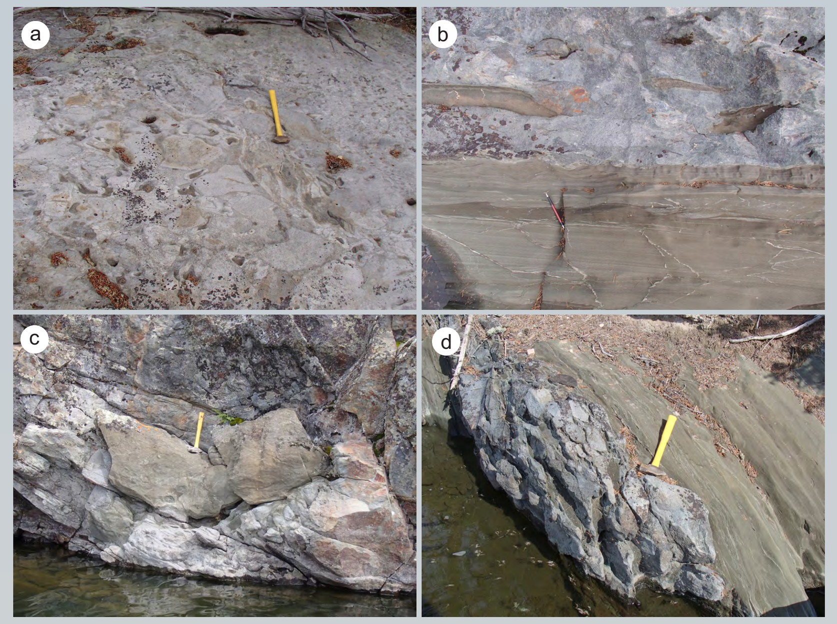

Figure 17: Outcrop photographs of dacitic volcanic conglomerate (DVC; ca. 2722 Ma; Corkery et al., 2000) interstratified with the UFA in the western bay: a) massive to crudely stratified, clast-supported DVC; b) sharp basal contact of DVC (top), showing mudstone rip-ups derived from the underlying UFA (bottom); c) DVC containing a large angular block of pebble conglomerate (below hammer) derived from the UFA; d) thin lens of DVC interstratified with the UFA.

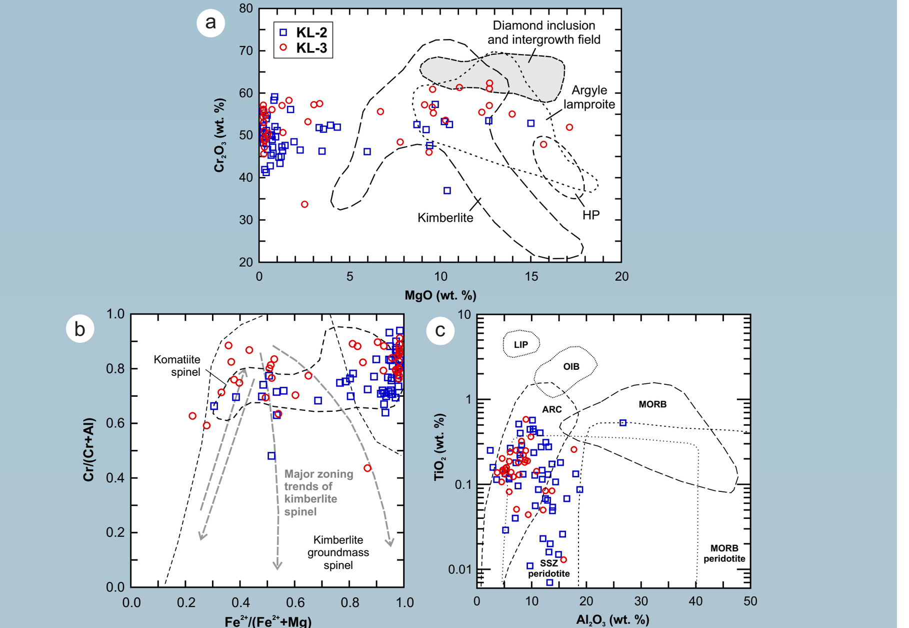

Figure 18: Bivariate plots for chromite and Cr-spinel grains recovered from MGS samples KL-2 and KL-3: a) MgO vs. Cr_2O_3; fields for diamond inclusions, Argyle lamproite and HP lamprophyre are from Fipke et al. (1995); field for kimberlite spinel is from Nowicki et al. (2007); b) $Fe^{2+}/(Fe^{2+}+Mg)$ vs. Cr/(Cr+Al); compositional field for komatiite spinel is from Barnes and Roeder (2001); compositional field and principal zoning trends for kimberlite groundmass spinel are from Roeder and Schulze (2008); c) Al_2O_3 vs. TiO_2 (after Kamenetsky et al., 2001). Abbreviations: ARC, island-arc; LIP, large igneous province; OIB, ocean-island basalt; MORB, mid-ocean–ridge basalt; SSZ, supra-subduction zone. Spinel compositions are consistent with typical arc volcanic rocks (including lamprophyre) or komatiite.

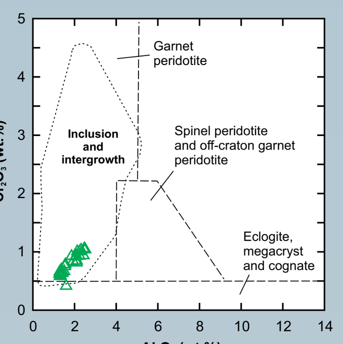

Figure 19: Bivariate plot (Al_2O_3 vs. Cr_2O_3) for Cr-diopside grains from MGS sample KL-3; compositional field for diamond-inclusion and diamond-intergrowth Cr-diopside is from Nimis (2002); other compositional fields are from Ramsay and Tompkins (1994).

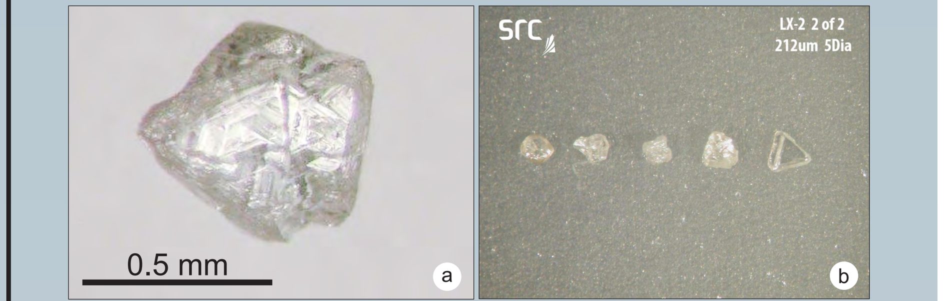

Figure 20: Microdiamonds (MD) recovered from MGS sample LX-2: a) MD from the +0.425 mm size fraction, showing minor inclusions; b) examples of clear, colourless MD from the +0.212 mm size fraction.

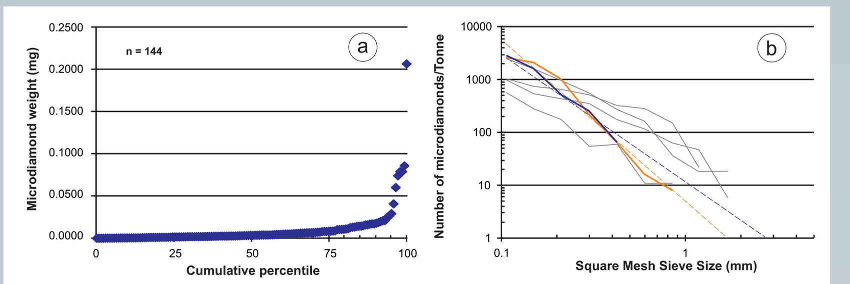

Figure 21: Distribution plots for microdiamonds (MD) from MGS sample LX-2 (15.8 kg): a) cumulative percentile plot of MD size by weight, showing a continuous distribution up to the 95th percentile; b) square-mesh sieve size vs. number of MD/tonne (log-log) showing a linear, relatively steep distribution curve for sample LX-2 (blue line; dashed line indicates best-fit); shown for comparison purposes are MD distribution curves (grey lines) for samples of resedimented volcaniclastic kimberlite from the Misery complex of the Ekati mine (Krebs et al., 2016); data from a continuous channel sample (12.9 m, 128kg) collected by Altius Minerals Corp. (press release, September 25, 2017; see **Figure 7** for channel location) across the discovery outcrop is indicated by the orange line (dashed line indicates best-fit); the conglomerate shows high concentrations of MD in the smaller size fractions, whereas the steep slopes of the best-fit lines suggest that the maximum stone size is likely to be ~2 mm.

Exploration implications

The southern Knee Lake microdiamond occurrence represents the first discovery of diamonds associated with alkaline volcanic rocks in Manitoba.

Although diamonds are typically hosted by kimberlite intrusions (e.g., Kjarsgaard, 2007), significant deposits and occurrences are also associated with other types of mantle-derived intrusions, including lamproite and ultramafic lamprophyre, and calcalkaline lamprophyre (e.g., Gurney et al., 2005). Examples of the latter association in the Michipicoten belt near Wawa, Ontario (Lefebvre et al., 2005), are strongly analogous to the Knee Lake diamond occurrence and provide insight into the potential complexity of these systems, with relevance to exploration methodologies.

As in the Michipicoten belt, discontinuous exposure and complex structure at Knee Lake hinder stratigraphic correlations of diamondiferous units. In addition, the type and chemistry of indicator minerals obtained from the diamondiferous rocks differ significantly from those recovered from surficial sediments (e.g., Fedikow et al., 2002), indicating derivation from different sources. At Knee Lake, drift prospecting is further complicated by a number of factors, including several directions of ice flow, widespread dilution of the local bedrock signature by far-travelled calcareous till, streamlined landforms that do not reflect the ice-flow transport direction, and a locally thick blanket of glaciolacustrine clay (Trommelen, 2015).

For these reasons, the initial stages of follow-up exploration should focus on detailed mapping of volcaniclastic, sedimentary and intrusive rocks of the ultramafic facies association, and the collection of well-constrained bedrock samples for caustic fusion and heavy mineral separation in order to establish the spatial distribution of diamondiferous rocks and the nature of their indicator mineral populations. In addition, an orientation survey of surficial sediments inland from the eastern and western bays, including the geochemical signature of the glacial till as per the recommendations of Trommelen (2015), as well as conventional geochemical analysis for elements known to be enriched in the ultramafic facies association rocks (e.g., Ba, Cr, Ni, Sr), may also prove valuable.

References

Anderson, S.D. 2016: Report of Activities 2016, Manitoba Geological Survey, p. 1–15.
Anderson, S.D. 2017a: Report of Activities 2017, Manitoba Geological Survey, p. 1–11.
Anderson, S.D. 2017b: Manitoba Geological Survey, Open File Report OF2017-3, 27 p.
Anderson, S.D., Kremer, P.D. and Martins, T. 2012: Report of Activities 2012, Manitoba Geological Survey, p. 6–22.
Anderson, S.D., Kremer, P.D. and Martins, T. 2013: Report of Activities 2013, Manitoba Geological Survey, p. 7–22.
Anderson, S.D., Syme, E.C., Corkery, M.T., Bailes, A.H. and Lin, S. 2015a: Manitoba Geological Survey, Preliminary Map PMAP2015-1, 1:20 000 scale.
Anderson, S.D., Syme, E.C., Corkery, M.T., Bailes, A.H. and Lin, S. 2015b: Report of Activities 2015, Manitoba Geological Survey, p. 9–23.
Barnes, S.J. and Roeder, P.L. 2001: Journal of Petrology, v. 42, p. 2279–2302.
Cabanis, B. and Lecolle, M. 1989: Comptes Rendus de l'Academie des Sciences, v. 309, p. 2023–2029.
Corkery, M.T., Cameron, H.D.M., Lin, S., Skulski, T., Whalen, J.B. and Stern, R.A. 2000: Report of Activities 2000, Manitoba Geological Survey, p. 129–136.
Fedikow, M.A.F., Nielsen, E., Conley, G.G. and Lenton, P.G. 2002: Manitoba Geological Survey, Open File Report OF2002-1.
Fipke, C.E., Gurney, J.J. and Moore, R.O. 1995: Geological Survey of Canada, Bulletin 423, 86 p.
Gilbert, H.P. 1985: Geological Services, Geological Report GR83-1B, 76 p.
Gurney, J.J., Helmstaedt, H.H., Le Roex, A.P., Nowicki, T.E., Richardson, S.H. and Westerlund, K.J. 2005: Economic Geology 100th Anniversary Volume, p. 143–177.
Kamenetsky, V.S., Crawford, A.J. and Meffre, S. 2001: Journal of Petrology, v. 42, p. 655–671.
Kjarsgaard, B.A. 2007: Geological Association of Canada, Mineral Deposits Division, Special Publication No. 5, p. 245–272.
Krebs, M.Y., Pearson, D.G., Stachel, T., Stern, R.A., Nowicki, T. and Cairns, S. 2016: Economic Geology, v. 111, p. 503–525.
Lefebvre, N., Kopylova, M. and Kivi, K. 2005: Precambrian Research, v. 138, p. 57–87.
Nimis, P. 2002: The Canadian Mineralogist, v. 40, p. 871–884.
Nowicki, T.E., Moore, R.O., Gurney, J.J. and Baumgartner, M.C. 2007: Developments in Sedimentology, v. 58, p. 1235–1267.
Pearce, J.A. and Peate, D.W. 1995: Annual Review of Earth and Planetary Sciences, v. 23, p. 251–285.
Peccerillo, A. and Taylor, S.R. 1976: Contribution to Mineralogy and Petrology, v. 58, p. 63–81.
Ramsay, R.R. and Tompkins, L.A. 1994: Proceedings of the 5th International Kimberlite Conference, Araxá, Brazil, Special Publication, v. 2, p. 329–345.
Roeder, P.L. and Schulze, D.J. 2008: Journal of Petrology, v. 49, p. 1473–1495.
Stott, G.M., Corkery, M.T., Percival, J.A., Simard, M. and Goutier, J. 2010: Ontario Geological Survey, Open File Report 6260, p. 20-1–20-10.
Sun, S-s. and McDonough, W.F. 1989: Geological Society of London, Special Publications, v. 42, p. 313–345.
Syme, E.C., Corkery, M.T., Bailes, A.H., Lin, S., Cameron, H.D.M. and Prouse, D. 1997: Report of Activities, 1997, Geological Services, p. 37–46.
Syme, E.C., Corkery, M.T., Lin, S., Skulski, T. and Jiang, D. 1998: Report of Activities, 1998, Geological Services, p. 88–95.
Trommelen, M.S. 2015: Manitoba Geological Survey, Geoscientific Paper GP2013-3, 30 p. plus 13 appendices.

Acknowledgments

J. Deyholos, D. Downie and M. Stocking (University of Manitoba) provided capable and enthusiastic assistance during the field mapping component of this study. The author benefited from discussions with R. Syme, T. Corkery and A. Chakhmouradian, and C. Böhm provided a thorough review of the manuscript. Mineral separation and analysis (microdiamonds and indicator minerals) was funded by Mount Morgan Resources Ltd. (M. Fedikow), Polaris Capital Ltd. (R. Day), Indicator Explorations Ltd. (J. Lee) and H. Westdal.